

Assessment of the Cherenkov camera alignment through Variance images for the ASTRI telescope

Simone Iovenitti · Giorgia Sironi · Enrico Giro · Alberto Segreto · Osvaldo Catalano · Milvia Capalbi

Received: date / Accepted: date

Abstract A peculiar aspect of Cherenkov telescopes is that they are designed to detect atmospheric light flashes on the time scale of nanoseconds, being almost blind to stellar sources. As a consequence, the pointing calibration of these instruments cannot be done in general exploiting the standard astrometry of the focal plane. In this paper we validate a procedure to overcome this problem for the case of the innovative ASTRI telescope, developed by INAF, exploiting sky images produced as an ancillary output by its novel Cherenkov camera. In fact, this instrument implements a statistical technique called “Variance method” (VAR) owning the potentiality to image the star field (angular resolution $\sim 11'$). We demonstrate here that VAR images can be exploited to assess the alignment of the Cherenkov camera with the optical axis of the telescope down to $\sim 1''$. To this end, we evaluate the position of the stars with sub-pixel precision thanks to a deep investigation of the convolution between the point spread function and the pixel distribution of the camera, resulting in a transformation matrix that we validated with simulations. After that, we considered the rotation of the field of view during long observing runs, obtaining light arcs that we exploited to investigate the alignment of the Cherenkov camera with high precision, in a procedure that we have already tested on real data.

The strategy we have adopted, inherited from optical astronomy, has never been performed on Variance images from a Cherenkov telescope until now, and it can be crucial to optimize the scientific accuracy of the incoming MiniArray of ASTRI telescopes.

Keywords Cherenkov astronomy · Pointing · Tracking · Variance method · Alignment

Simone Iovenitti
Università degli Studi di Milano
INAF-Osservatorio Astronomico di Brera
E-mail: simone.iovenitti@inaf.it

1 Introduction

ASTRI-Horn is a Cherenkov telescope entirely developed by the Istituto Nazionale di Astrofisica (INAF), aiming at the study of very-high energy (VHE) cosmic radiation, up to 100 TeV and beyond [17]. It is a prototype instrument both for the realization of the ASTRI MiniArray observatory and for the opto-mechanical structure of Small-Sized Telescopes (SST) to be implemented in the Cherenkov Telescope Array (CTA) [6]. ASTRI-Horn is an example of Imaging Atmospheric Cherenkov Telescope (IACT) [10], designed to detect nanosecond light flashes due to the interaction of the incoming cosmic radiation with the atmosphere. In particular, ASTRI-Horn presents some peculiar novelties that make it a unique telescope in its genre, as it is briefly discussed hereafter.

ASTRI-Horn is the first Cherenkov telescope with a dual-mirror configuration [1] (a modified Schwarzschild-Couder design [7]), allowing to have a wide, aplanatic field of view (FoV) up to 10.5° diameter, with a primary mirror raw aperture of about 4.3 m, despite a short equivalent focal length of ~ 2.15 m [19]. This optical scheme presents a small plate-scale (37.5 mm/deg), allowing to use miniaturized Silicon Photo-Multipliers sensors (SiPM) in the focal plane, sized on purpose to couple with the point spread function (PSF, ~ 7 mm) of the instrument [7]. Each SiPM constitutes a square pixel covering $\sim 11.2'$ in the sky, with sensitivity in the range of wavelengths between 300 and 550 nm with an appropriate filter. Globally, the whole camera is a mosaic of 37 tiles, called Photon Detection Modules (PDM), each composed of 64 pixels [3]. However, ASTRI-Horn operated with a reduced PDM configuration of only 21 tiles, corresponding to $\sim 7.5^\circ$, in order to carry out the instrument performance validation.

The primary output of the camera are the images of nanosecond atmospheric Cherenkov flashes, produced by the incoming VHE cosmic radiation. From this data stream, all the scientific information about astrophysical quantities can be retrieved, using the Hillas parametrization [9] and suitable Monte Carlo simulations to analyze the shape of the flashes. The stellar component of the night sky background light is almost invisible in this output, as the electronics was specifically designed to filter any steady or slow-varying incoming signal, as they are not of interest for the Cherenkov data reduction. However, differently from other Cherenkov detectors, the ASTRI camera actually owns the potentiality to image the star field, with an ancillary output which is proportional to the incoming photon flux over every pixel, exploiting a statistical technique implemented in the logic board: the Variance method¹. It is based on the analysis of the electric signal detected by the camera front-end electronics, sampling randomly the output of the pixels not triggered by the Cherenkov events. The net result is, for each pixel, a sequence of values whose average is constant with time, but whose variance is proportional to the flux on the pixel [3]. This technique is inherited from the photo-multipliers tube technology and with the ASTRI project it has been applied for the first time to a Cherenkov telescope equipped with SiPM sensors. Using the Variance data, we can monitor the night sky background light and access the position of the stars in the field of view, opening the intriguing possibility to

¹ The innovative Cherenkov camera CHEC [22], recently developed, can also produce sky images exploiting a technique similar to the Variance, but using a separate DC coupled line to extract (integrate) the signal [21].

assess the actual pointing of the telescope without requiring any auxiliary optical instrument as every other IACT does [18].

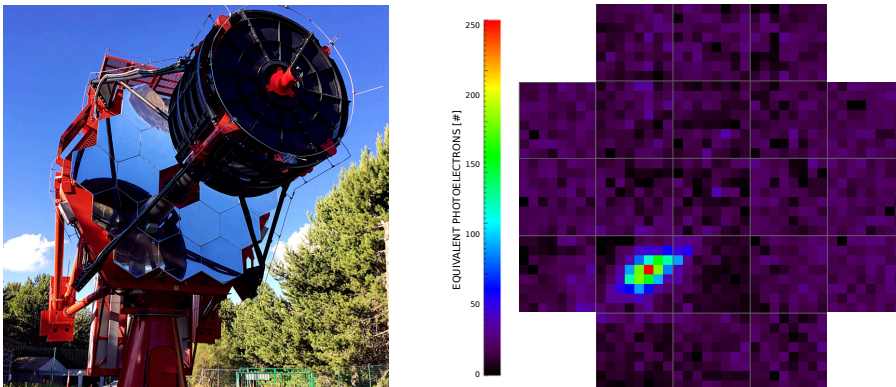


Fig. 1: The ASTRI-Horn prototype telescope (left) and a typical Cherenkov event detected by the SiPM camera (right): no stars are visible in scientific images.

1.1 Scope of this work

The pointing direction of the ASTRI Cherenkov SiPM camera cannot be assessed through the use of images taken directly with it, because the acquisition electronics filters out the steady or slow-varying component of the sky light and hence the star field cannot be adopted as a reference. For this reason, it is difficult to measure any eventual undesired effect introducing a mis-pointing of the camera system, e.g. mechanical tolerances or gravity flexures. Despite this, in this paper we validate a method to measure the position of the camera geometric center with respect to the actual telescope optical axis pointing direction, exploiting the apparent motion of stars into Variance images. To this end, the main challenge is to achieve the angular resolution necessary for scientific objectives (tens of arcseconds), despite the large pixel size (few arcminutes) and the non-uniform gaps between the tiles of the Cherenkov camera [3]. To overcome these problems, we adopted a very common approach: to study the behaviour of the PSF as it crosses the pixels during the apparent rotation of the field of view due to the sidereal motion and the alt-azimuthal mount of the telescope [18]. This technique is often adopted in optical astronomy [16], but it has never been performed on data from a Cherenkov camera, until now.

In this work we demonstrate that, in the case of ASTRI, provided at least 4 bright stars ($\lesssim 5.5$ mag) in the FoV it is possible to verify the alignment of the Cherenkov camera with the optical axis of the telescope with a precision down to $\sim 1''$. To this end, we developed a pipeline to analyse the star trails (section 4) using an algorithm to retrieve the position of stars with sub-pixel accuracy (section 3). We validated our procedure through simulations, then we applied it to real data taken with ASTRI-Horn. Figure 2 shows a flowchart of the whole procedure, while section 5

contains a discussion of the results, together with the future improvements to implement it in the ASTRI MiniArray.

To begin, section 2 starts with the sample selection.

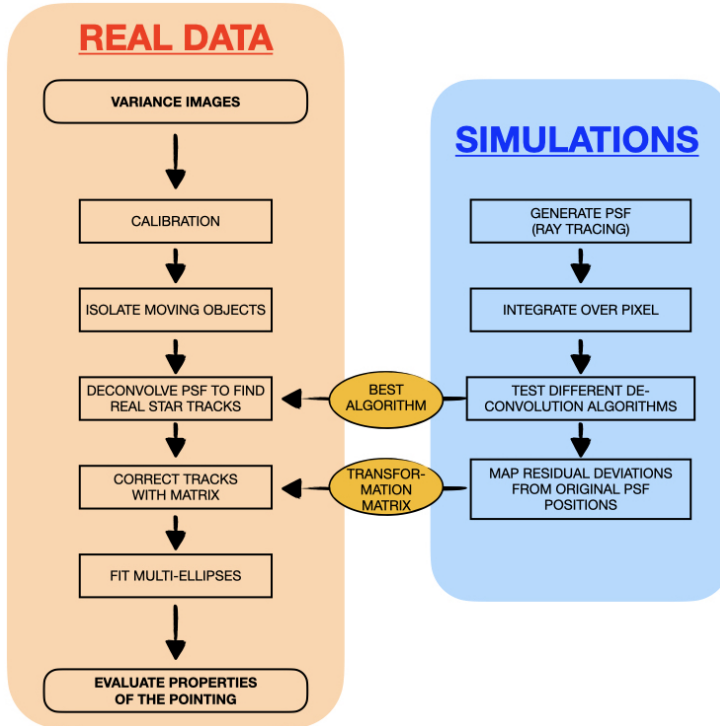


Fig. 2: Flowchart of the procedure presented in this paper.

2 Data selection and pre-processing

Variance data are taken in parallel to scientific data, during every observing run of the telescope. In particular, the electronics of ASTRI-Horn was configured to generate a Variance image, or *frame*, every ~ 3.25 s. In these images, the brightest stars ($\lesssim 5.5$ mag) are clearly visible and they present the typical FoV rotation of every telescope with an alt-azimuthal mount performing a tracking observation, as it is reported in the next section. In order to analyse the trajectories of the stars in the FoV, only the observing runs with the largest rotation must be selected among the data collected by ASTRI-Horn². After that, images must be calibrated with a flat-field-like procedure. Finally, pixels containing stars must be isolated for the detailed analysis.

² As a prototype telescope, ASTRI-Horn accomplished only one full observing campaign, pointing at the Crab Nebula region, taking data in ON/OFF mode [13].

2.1 Rotation of the field of view

The angular extension of the FoV rotation can be calculated considering that it is given by the evolution of the *parallactic angle* η , i.e. the angle between the north celestial pole and the zenith, with the vertex in the pointing direction [8]. At any time, during a tracking observation of an object, the value of η is given by [5]

$$\frac{\sin \eta}{\sin \left(\frac{\pi}{2} - \phi \right)} = \frac{\sin h}{\sin z}, \quad (1)$$

where ϕ is the telescope’s latitude, h is the object’s hour angle and z is the object’s zenith angle, that we can retrieve from the position of the telescope motors’ encoders. The time dependence is embedded into h and z , and there is not a simple relation between the amplitude of the rotation $\Delta\eta$ and the time length of the observing run³. To test our procedure, we selected those cases where the telescope was in tracking mode and $\Delta\eta \geq 25^\circ$ among all the data sets available in the ASTRI-Horn archive: we identified 9 observing runs⁴. Among them, only 2 cases present at least 4 bright stars in the FoV and we chose them to test our procedure. Table 1 report their parameters.

Run ID	Date	Pointing	Frames	Time lenght	Angular coverage
1597	2019-02-26	Crab Nebula	2275	1h 59m 44s	33.4°
1620	2019-02-28	Crab Nebula	1986	1h 43m 39s	25.5°

Table 1: Parameters of observing runs that we considered as test-case.

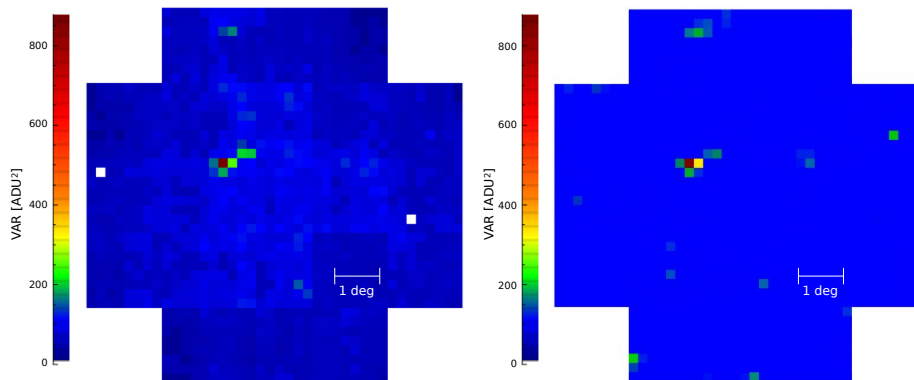


Fig. 3: Visualization of the Variance data taken with the ASTRI-Horn Cherenkov camera before (left) and after (right) the flat-field calibration. Local maxima are stars in the FoV, the brightest one is *Tianguan* or Zeta Tauri (123 Tau). Observing run 1597 (see table 1).

³ For simulating in details the FoV rotation we adopted the software “Star Coverage” [12].

⁴ In principle, consecutive runs on the same target can be concatenated for our analysis, thus increasing the total angular coverage, but for testing the procedure we decided to work on *single* runs only.

2.2 Gain calibration

The pixel values in the Variance images must undergo a gain-calibration process (flat field) whose parameters has unfortunately not been characterized in laboratory yet⁵. Thus, we performed the calibration adopting a statistical approach: for every pixel, we consider the median Variance level in every run (in order to mitigate the effect of the star spots occasionally transiting over some pixels in some frames) and then we take the average of these values over our sample of 9 long observing runs. Hence, the calibration coefficient C_i for every pixel x_i is given by

$$C_i = \frac{1}{N} \sum_{\text{RUNS}} \text{median}(x_i, f), \quad (2)$$

where f is the set of frames composing every observing run and N is their number. The final calibration factor F_i is given by the inverse of C_i , after an appropriate normalization, and the pixel value in every frame is finally calculated with $x_i \times F_i$. Figure 3 shows the effects of this calibration.

2.3 Identify the stars

During the rotation of the FoV the image of every star changes position on the camera, thus increasing the “variance of the Variance” of the pixels receiving light. As a consequence, considering for each pixel the standard deviation of the whole observing run, we can visualize the star trails, as it is shown in figure 4 for the observing run 1597. After that, a clustering algorithm (centroid-based, of the *k-means* family [4]) isolates the groups of pixels belonging to the same moving spot, hence identifying the tracks of the brightest stars. In the following part of the analysis, only pixels within the clusters will be considered to retrieve the position of the stars in every frame.

3 Retrieve the position of stars

In order to draw the track of the stars in the FoV with sufficient precision (few arcminutes), their position in every frame must be determined with sub-pixel accuracy. Unfortunately, the shape of the PSF cannot be exploited to this aim, because its average extension is almost equal to the pixel size (~ 7 mm) [6]. However, when the star spot falls across multiple pixels, it is possible to retrieve the position of the centroid considering their different illumination, i.e. the PSF convolution over the pixel distribution (see figure 5). To this end, we simulated the pixel illumination by a generic celestial point-source and we tested different de-convolution algorithms using the dispersion from the original star position as a figure of merit (section 3.1). Moreover, we improve this result studying in detail the effect of the gaps between the pixels (section 3.2).

⁵ By now, the full calibration of the camera was performed only for scientific data [11].

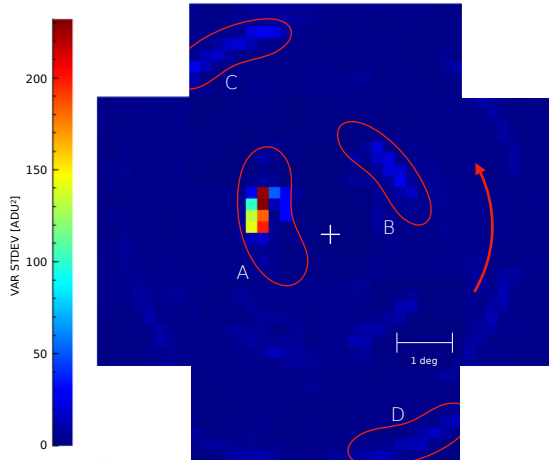


Fig. 4: Star trails isolated by the clustering algorithm. Camera center is pointing the Crab Nebula. Star A is 123 Tau (*Tianguan*, 3.0 mag), B is 114 Tau (4.8 mag), C is 119 Tau (4.3 mag) and D is 125 Tau (5.2 mag) [values taken from SIMBAD, V band].

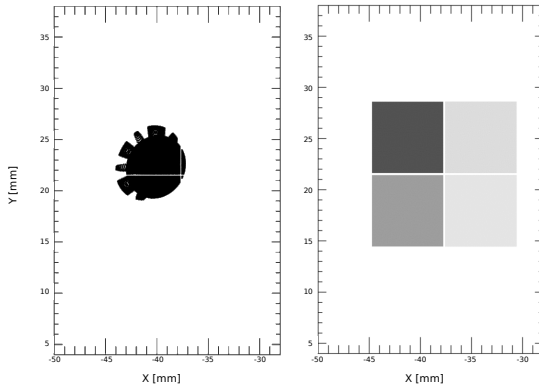


Fig. 5: Ray-tracing simulation of 83518 photons from a point-like source 1.25° off the optical axis of the telescope. *Left*: the resulting PSF of the ASTRI-Horn telescope. *Right*: the convolution of that PSF over the Cherenkov camera pixels. The gray scale is proportional to the number of photons collected by every pixel, while the white separation lines represent the gaps between them.

3.1 Deconvolution of the PSF

In order to choose the best algorithms to de-convolve the PSF from the Variance images, we started simulating the whole process of image creation in the ASTRI camera. We artificially generated a celestial point-source off axis and performed a full ray-tracing of 83 518 photons to produce its theoretical spot onto the camera⁶. Then we considered its apparent motion due to the evolution of the parallactic

⁶ The procedure to simulate the PSF was validated with direct measurements during the commissioning phase of the ASTRI-Horn telescope [6].

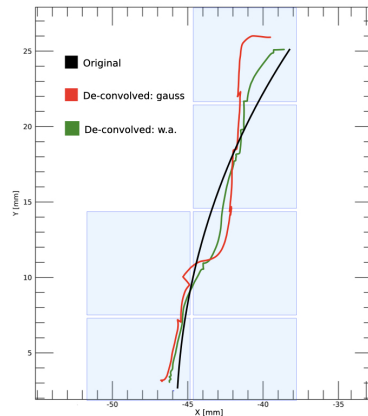


Fig. 6: Track of the PSF centroid of the original simulated star (black) and its reconstruction with different algorithms after the integration of light over the pixels. The time length of the simulation is 2 h. Light blue squares represent six pixels of the camera.

angle η , given by equation 1. We integrated light spots over the camera pixel area, obtaining a Variance-like set of images. Finally, we tested different strategies to recover the position of the original spot centroid, evaluating their accuracy via the standard deviation δ of the reconstructed points with respect to the initial simulated trail⁷.

- *Gaussian fit (Gauss)*, $\delta = 2.39'$. The Variance value of every pixel is assigned to the position of the pixel center and the resulting matrix is interpolated to obtain an image; every local maximum is fitted with a 2D-Gaussian function to obtain the centroid position.
- *Weighted-average (W.A.)*, $\delta = 0.81'$. Within each cluster (see sec. 2.3), we consider the pixel with the maximum value together with its eight nearest neighbor⁸: the barycenter of the simulated light spot is given by the average of pixels center positions, weighted by the recorded intensities.

Figure 6 shows the outcome of the two methods described: W.A. presents a better match with the original curve, so this method was adopted, as it requires fewer further corrections to retrieve the original star trail. In addition, figure 6 also presents little jumps close to the gaps between the pixels, suggesting that their role must be studied in details: they will be considered in section 3.2.

3.2 Effects of gaps between pixels

Gaps between pixels subtract photons to the star spots, modifying the shape of the PSF and distorting the outcome of the deconvolution algorithm⁹. This effect

⁷ δ is measured in mm and converted in arc-minutes using the plate-scale.

⁸ Using 9 pixels in total we are sure to consider also the tails of the PSF.

⁹ The loss of photons is negligible for the analysis of the Cherenkov showers, as they typically cover a total surface made of several pixels, while dead areas are very small in comparison.

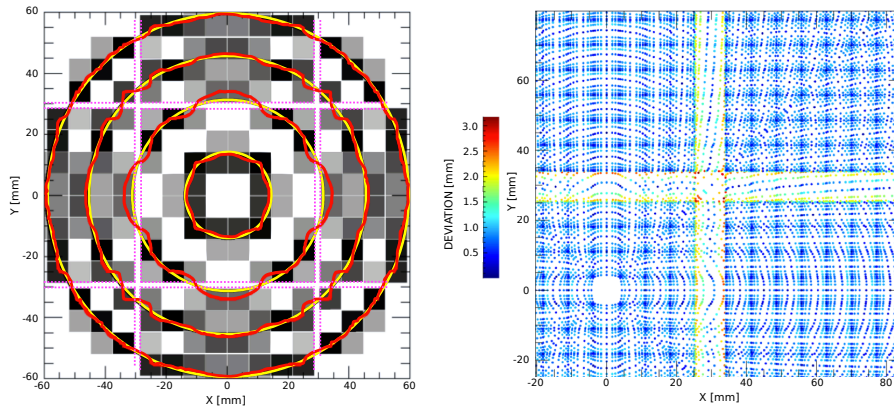


Fig. 7: Left: central portion of the ASTRI-Horn camera with the simulation of the tracks of 4 stars rotating along perfect circles (360°). The reconstruction of the tracks (red line) presents considerable deviations from the theoretical curve (yellow) when the spot crosses the gap between PDMs (magenta). The grey scale of the pixels is proportional to their illumination. Right: each point represents the position of a star centroid retrieved by our algorithm and the color scale expresses its displacement from the theoretical position.

is enhanced at the edge of PDMs, where the gap is larger (0.8 to 1.6 mm) compared with the gap between “internal” pixels (0.2 mm) [2]. Figure 7 highlights this phenomenon, with a virtual FoV rotation of 360° .

In order to characterize and remove the effect of pixel gaps, we simulated a PSF in every point of a fine grid of possible positions in the camera and we measured the distance between the original spot centers and the ones calculated with the deconvolution algorithm (*W.A.*). We obtained a map of the distortion introduced by the geometry of the camera (reported in figure 7, right) that can be used as a transformation matrix to correct the position of calculated centroids. The effectiveness of this procedure is verified applying the transformation matrix on the track of figure 7, left (red line). The maximum deviation δ is reduced of about 40%.

4 Analysis of the real tracks observed by ASTRI-Horn

To take into account any possible deviation from the expected pattern, we assumed that the shape of the real star trails can lie along multiple arcs of ellipses with the same center, eccentricity and tilt angle, as it is shown in figure 8. To extract the parameters of the ellipses we fitted the data with a suitable function (section 4.1). Furthermore, we investigated the dependency of the results on the angular coverage, determining in which conditions our procedure can ensure the highest precision (section 4.2).

4.1 The fit procedure

The trails of the stars’ centroids are fitted with a function that we defined on purpose, describing simultaneously multiple ellipses, with the same center, eccen-

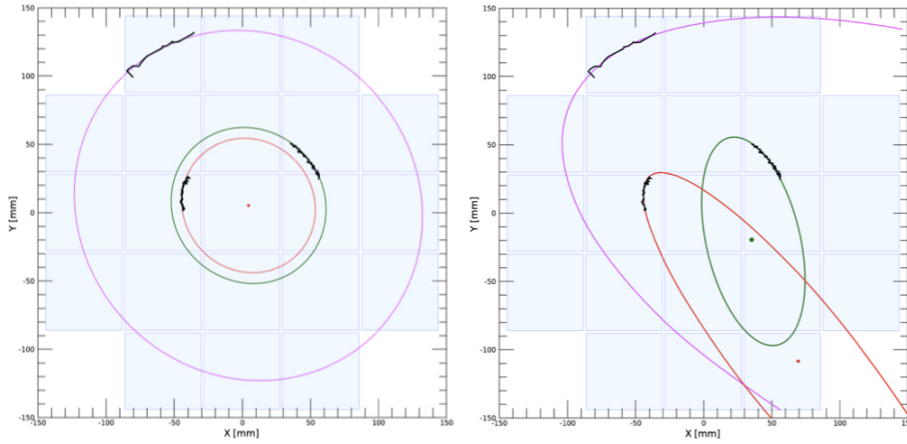


Fig. 8: Output of the fit described in section 4.1: star tracks from real Variance data are represented in black while light-blue squares represent PDMs of the ASTRI-Horn camera. *Left*: 3 stars were considered simultaneously for the fit; *right*: each star was fitted individually.

tricity and tilt angle. The fit was performed with the MPFIT procedure of the IDL library [14]. The number of free parameters is $p = 4 + n$, where n is the number of stars. In particular, the parameters of the fitting functions are

- X_0 and Y_0 of the center;
- θ tilt angle;
- major and minor semiaxes of the innermost elliptical star trail;
- major semiaxis of the other elliptical star trails.

The fit function is called several times, with random changes to the initial parameters and without constraints: the dispersion of the results is adopted as an estimation of their uncertainty. Figure 8 reports the mean of fit results for the observing run 1597, with 3 stars considered simultaneously in the trail fitting procedure. In this example, the center of the ellipse is in $X_0 = (4.51 \pm 0.06)$ mm, $Y_0 = (5.25 \pm 0.37)$ mm, equivalent to an angular distance of $\delta_0 = (10.6 \pm 0.5)''$ from the geometric center of the camera¹⁰. However, considering four stars for the analysis, hence constraining the fit, the results becomes consistent with the geometric center of the camera, with an error lower than $1''$. This behaviour is shown and discussed in the next section.

4.2 Results

The dispersion of fit results strongly depends on the number of stars considered and their angular coverage, as it is reported in figure 9. In particular, when less than 4 stars are included, the fit result is influenced by the edgy shape of the star-trail reconstruction, due to the large pixel size. An example is reported in figure 8 *right*,

¹⁰ Uncertainties in the x and y directions are evaluated independently: the error on X_0 is smaller as the data-set considered here provides a better coverage of the horizontal direction.

where the stars are fitted individually and the outcome is non-realistic, too far from the expected circular shape. We investigated this effect performing our analysis on the observing runs selected in table 1, both presenting 4 bright stars, allowing us to consider different combinations of 2 stars (6), 3 stars (4) and 4 stars (1), per each of them. Results are reported in figure 9, showing the distance of their calculated centroids from the camera geometric center, with their errors. Table 2 reports a summary of this analysis.

Stars [num]	Distance from center ["]	Error ["]
2	1689	620
3	73	33
4	0.1	< 1.0

Table 2: Averages of fits results and their error, for the analysis with 2, 3 and 4 stars, on the real data from table 1.

It emerges that it is sufficient to have 4 bright stars in the FoV (like in the case of the Crab Nebula region) to obtain a measure of the offset between the telescope axis and the geometric center of the Cherenkov camera with an uncertainty lower than 1". In fact, with 4 stars the fit procedure is well constrained and hence reliable, providing us a result which is exploitable for scientific purpose.

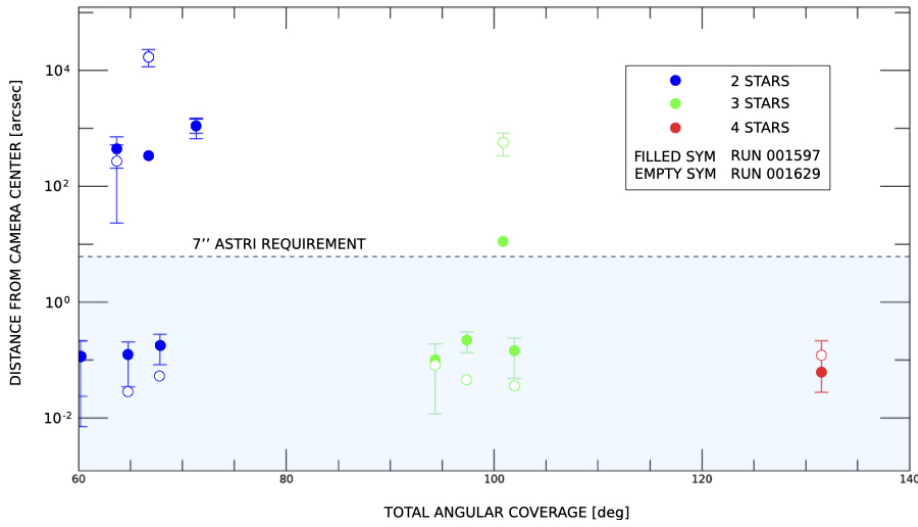


Fig. 9: Dispersion of fits results and their error, for combinations of 2,3 and 4 stars, from the two observing runs of table 1 (denoted with filled and empty symbols). In abscissa there is the total angle covered by the sum of the stars considered for the fit during FoV rotation.

The 7" value for the pointing precision requirement of a single ASTRI telescope [20] is reported as a reference.

5 Conclusion

Variance images represent a unique opportunity to study the sky portion actually framed by the Cherenkov camera of the ASTRI-Horn telescope, owning the potentiality to finely calibrate and monitor its pointing [18]. In particular, the procedure presented in this paper reveals any possible offset in the alignment of the Cherenkov camera with the optical axis of the telescope, exploiting the technique of the FoV rotation that was never applied before to real images from a Cherenkov camera. We validated our method with simulated star trails and, analysing real data taken by ASTRI-Horn, we demonstrated that its sensitivity is high enough to be exploited for scientific purpose, reaching the scale of arc-seconds if the FoV rotation is greater than 25° and 4 bright stars ($\lesssim 5.5$ mag) are present.

This work represents the first scientific analysis performed on real Variance data from an IACT and constitutes a powerful diagnostic tool to assess its pointing properties, hence optimizing the scientific accuracy of the whole system.

Lastly, we want to point out that applying our technique on a wider data sample by ASTRI-Horn one could in principle verify the alignment of the Cherenkov camera during all the different campaigns of the observing period¹¹, possibly enhancing the fine pointing reconstruction *post-facto*. On the other hand, in the incoming MiniArray of ASTRI telescopes, the procedure presented in this work will be implemented since the first calibration phase, assessing the alignment of the camera mount systems from the beginning [15].

5.1 Possible limitations of this method

At a first sight, the procedure we have presented for the alignment of the Cherenkov camera seems to require some very lucky conditions: no clouds along all the path of stellar sources during long acquisitions and a pretty crowded star field in the FoV in order to have a reliable reconstruction of the rotation. Actually, in real use cases passing clouds are not a problem, as it is not necessary that long star trails are continuous: several consecutive segments can be attached together and the fit procedure will be well constrained regardless to possible "holes" in the middle. On the other hand, to have 4 bright stars at least in the FoV is not so common, despite the large aperture of the ASTRI telescope. However, it is essential to point out that this alignment procedure of the camera will not be performed every night, but only on dedicated calibration sessions or in case of necessity [15], and suitable sky regions will be chosen in those occasions.

Regardless to the pointing direction, nowadays the sky view is full of bright satellites. Their presence can alter the reconstruction of the stars' position in our procedure, but fortunately in a negligible way. In fact, even high altitude satellites are very fast compared to the diurnal motion, and hence their light can affect the reconstruction of each star centroid for no more than ten point maximum along its track.

Possible important limitations of our method are represented by distortions in the star trails introduced by external agents, e.g. strong wind gusts (but the weather

¹¹ We remind that ASTRI-Horn is a prototype telescope, and often extraordinary maintenance operations were performed between different observing campaigns, also regarding the camera mount system.

station would record their critical values), or the presence of errors in the tracking (for example a drift due to errors in the pointing model or to the motors inertia): this effect would influence the result of our analysis in a way that is difficult to simulate in advance. To overcome this problem the first solution is to execute the calibration with our procedure when the telescope is staring-mode pointing at Polaris, avoiding artifacts introduced by the movement of the structure. Secondly, another solution is to monitor constantly, frame by frame, the pointing direction of the telescope with very high precision, so to exclude possible tracking errors. To this end, we have already developed¹² a tool to analyze the position of known stars in the FoV and to compare the Variance data with the log of the motors' encoders and the images from an optical auxiliary device: the Pointing Monitoring Camera (PMC)¹³. This will ensure a robust and continuous monitoring of the pointing performances, so that the alignment of the Cherenkov camera can be investigated at a deep level with the procedure presented here, both during the assembly verification phase and dedicated calibration sessions.

Acknowledgements We remember that this work is supported by the Italian Ministry of Education, University, and Research (MIUR) with funds specifically assigned to the Italian National Institute for Astrophysics (INAF). This article has gone through internal ASTRI review and we want to thank all the members of that commission. In particular, we would like to thank Giovanni Pareschi, PI of the experiment, for the constant supervision and for his helpful corrections in the manuscript.

References

1. Canestrari, R., Catalano, O., Fiorini, M., Giro, E., La Palombara, N., Pareschi, G., Stringhetti, L., Tosti, G., Vercellone, S., Astri Collaboration, Martelli, F., Parodi, G., Rossettini, P., Tomelleri, R.: The ASTRI SST-2M Prototype: Structure and Mirror. p. 2913 (2013). URL <http://adsabs.harvard.edu/abs/2013ICRC...33.2913C>
2. Capalbi, M., Maccarone, M.C.: Geometry of the Focal Surface Camera. Internal Technical Report ASTRI-DES-IASFPA-3200-008, INAF-IASFPA (2017)
3. Catalano, O., Capalbi, M., Gargano, C., Giarrusso, S., Impiombato, D., Rosa, G.L., Maccarone, M.C., Mineo, T., Russo, F., Sangiorgi, P., Segreto, A., Sottile, G., Biondo, B., Bonanno, G., Garozzo, S., Grillo, A., Marano, D., Romeo, G., Scuderi, S., Canestrari, R., Conconi, P., Giro, E., Pareschi, G., Sironi, G., Conforti, V., Gianotti, F., Gimenes, R.: The ASTRI camera for the Cherenkov Telescope Array. In: Ground-based and Airborne Instrumentation for Astronomy VII, vol. 10702, p. 1070237. International Society for Optics and Photonics (2018). DOI 10.1117/12.2314984. URL <https://www.spiedigitallibrary.org/conference-proceedings-of-spie/10702/1070237/The-ASTRI-camera-for-the-Cherenkov-Telescope-Array/10.1117/12.2314984.short>
4. Everitt, B., Landau, S., Leese, M., Stahl, D.: Cluster Analysis, 5 edn. Wiley Series in Probability and Statistics. Wiley (2011). URL <https://www.wiley.com/en-us/Cluster+Analysis%2C+5th+Edition-p-9780470749913>
5. Filippenko, A.V.: THE IMPORTANCE OF ATMOSPHERIC DIFFERENTIAL REFRACTION IN SPECTROPHOTOMETRY. Publications of the Astronomical Society of the Pacific **94**(560), 715 (1982). DOI 10.1086/131052. URL <https://iopscience.iop.org/article/10.1086/131052/meta>. Publisher: IOP Publishing
6. Giro, E., Canestrari, R., Bruno, P., Catalano, O., Fugazza, D., Palombara, N.L., Maccarone, M.C., Pareschi, G., Russo, F., Scuderi, S., Segreto, A., Sironi, G., Tosti, G., Marchiori, G., Busatta, A., Marcuzzi, E., Folla, I.: The ASTRI-Horn

¹² Paper in preparation.

¹³ An auxiliary optical camera installed behind the secondary mirror, on the optical axis of the telescope (compatibly with gravity flexions and mechanical tolerances).

- telescope validation toward the production of the ASTRI Mini-Array: a proposed pathfinder for the Cherenkov Telescope Array. In: *Optics for EUV, X-Ray, and Gamma-Ray Astronomy IX*, vol. 11119, p. 111191E. International Society for Optics and Photonics (2019). DOI 10.1117/12.2530896. URL <https://www.spiedigitallibrary.org/conference-proceedings-of-spie/11119/111191E/The-ASTRI-Horn-telescope-validation-toward-the-production-of-the/10.1117/12.2530896.short>
7. Giro, E., Canestrari, R., Sironi, G., Antolini, E., Conconi, P., Fermino, C.E., Gargano, C., Rodeghiero, G., Russo, F., Scuderi, S., Tosti, G., Vassiliev, V., Pareschi, G.: First optical validation of a Schwarzschild Couder telescope: the ASTRI SST-2M Cherenkov telescope. *Astronomy & Astrophysics* **608**, A86 (2017). DOI 10.1051/0004-6361/201731602. URL <http://arxiv.org/abs/1709.08418>. ArXiv: 1709.08418
 8. Green, R.M., Green, R.M.: *Spherical Astronomy*. Cambridge University Press (1985). Google-Books-ID: wOpaUFQFwTwC
 9. Hillas, A.M.: Cerenkov light images of EAS produced by primary gamma **3** (1985). URL <http://adsabs.harvard.edu/abs/1985ICRC...3..445H>. Conference Name: 19th International Cosmic Ray Conference (ICRC19), Volume 3
 10. Hillas, A.M.: Evolution of ground-based gamma-ray astronomy from the early days to the Cherenkov Telescope Arrays. *Astroparticle Physics* **43**, 19–43 (2013). DOI 10.1016/j.astropartphys.2012.06.002. URL <http://www.sciencedirect.com/science/article/pii/S0927650512001326>
 11. Impiombato, D., Catalano, O., Giarrusso, S., Mineo, T., Rosa, G.L., Gargano, C., Sangiorgi, P., Segreto, A., Sottile, G., Bonanno, G., Garozzo, S., Grillo, A., Marano, D., Romeo, G., Gimenes, R.: Procedures for the relative calibration of the SiPM gain on ASTRI SST-2M camera. *Experimental Astronomy* **43**(1), 1–17 (2017). DOI 10.1007/s10686-016-9516-z. URL <http://link.springer.com/10.1007/s10686-016-9516-z>
 12. Iovenitti, S.: “Star coverage”, a simple tool to schedule an observation when FOV rotation matters. In: *Proceedings of 37th International Cosmic Ray Conference — PoS(ICRC2021)*, vol. 395, p. 735. SISSA Medialab (2021). DOI 10.22323/1.395.0735
 13. Lombardi, S., Catalano, O., Scuderi, S., Antonelli, L.A., Pareschi, G., Antolini, E., Arrabito, L., Bellassai, G., Bernlöhr, K., Bigongiari, C., Biondo, B., Bonanno, G., Bonnoli, G., Böttcher, G.M., Bregeon, J., Bruno, P., Canestrari, R., Capalbi, M., Caraveo, P., Conconi, P., Conforti, V., Contino, G., Cusumano, G., de Gouveia Dal Pino, E.M., Distefano, A., Farisato, G., Fermino, C., Fiorini, M., Frigo, A., Gallozzi, S., Gargano, C., Garozzo, S., Gianotti, F., Giarrusso, S., Gimenes, R., Giro, E., Grillo, A., Impiombato, D., Incorvaia, S., La Palombara, N., La Parola, V., La Rosa, G., Leto, G., Lucarelli, F., Maccarone, M.C., Marano, D., Martinetti, E., Miccichè, A., Millul, R., Mineo, T., Nicotra, G., Occhipinti, G., Pagano, I., Perri, M., Romeo, G., Russo, F., Sacco, B., Sangiorgi, P., Saturni, F.G., Segreto, A., Sironi, G., Sottile, G., Stammer, A., Stringhetti, L., Tagliaferri, G., Tavani, M., Testa, V., Timpanaro, M.C., Toso, G., Tosti, G., Trifoglio, M., Umana, G., Vercellone, S., Zanmar Sanchez, R., Arcaro, C., Bulgarelli, A., Cardillo, M., Cascone, E., Costa, A., D’Aì, A., D’Ammando, F., Del Santo, M., Fioretti, V., Lamastra, A., Mereghetti, S., Pintore, F., Rodeghiero, G., Romano, P., Schwarz, J., Sciacca, E., Vitello, F.R., Wolter, A.: First detection of the Crab Nebula at TeV energies with a Cherenkov telescope in a dual-mirror Schwarzschild-Couder configuration: the ASTRI-Horn telescope. *Astronomy & Astrophysics* **634**, A22 (2020). DOI 10.1051/0004-6361/201936791. URL <https://www.aanda.org/10.1051/0004-6361/201936791>
 14. Markwardt, C.B.: Non-linear Least-squares Fitting in IDL with MPFIT p. 4
 15. Mineo, T., Maccarone, M.C., Antonelli, L.A., Ambrosino, F., Bruno, P.G., Bulgarelli, A., Compagnino, A.A., Capalbi, M., Catalano, O., Centrone, M., Di Paola, A., Faccini, M., Giarrusso, S., Giordano, V., Impiombato, D., Iovenitti, S., Leto, G., Lombardi, S., Lucarelli, F., Mollica, D., Pareschi, G., Parmiggiani, N., Righi, C., Sangiorgi, P., Scuderi, S., Segreto, A., Sironi, G., Sottile, G., Speziali, R., Tosti, G., Zampieri, L.: Tools and Procedures for the ASTRI Mini-Array Calibration. In: *Proceedings of 37th International Cosmic Ray Conference — PoS(ICRC2021)*, vol. 395, p. 197. SISSA Medialab (2021). DOI 10.22323/1.395.0197
 16. Rodeghiero, G., Arcidiacono, C., Pott, J.U., Perera, S., Pariani, G., Magrin, D., Riechert, H., Glück, M., Gendron, E., Massari, D., Sauter, J., Fabricius, M., Häberle, M., Meßlinger, S., Davies, R., Ciliegi, P., Lombini, M., Schreiber, L.: Performance and limitations of using ELT and MCAO for 50 uas astrometry. In: *Ground-based*

- and Airborne Instrumentation for Astronomy VIII, vol. 11447, p. 114471Z. International Society for Optics and Photonics (2020). DOI 10.1117/12.2560373. URL <https://www.spiedigitallibrary.org/conference-proceedings-of-spie/11447/114471Z/Performance-and-limitations-of-using-ELT-and-MCAO-for-50/10.1117/12.2560373.short>
17. Scuderi, S.: From the Etna volcano to the Chilean Andes: ASTRI end-to-end telescopes for the Cherenkov Telescope Array. In: Ground-based and Airborne Telescopes VII, vol. 10700, p. 107005Z. International Society for Optics and Photonics (2018). DOI 10.1117/12.2312453. URL <https://www.spiedigitallibrary.org/conference-proceedings-of-spie/10700/107005Z/From-the-Etna-volcano-to-the-Chilean-Andes--ASTRI/10.1117/12.2312453.short>
 18. Segreto, A., Catalano, O., Maccarone, M.C., Mineo, T., La Barbera, A., Cta Astri Project, F.T.: Calibration and monitoring of the ASTRI-Horn telescope by using the night-sky background measured by the photon-statistics ("variance") method. p. 791 (2019). URL <http://adsabs.harvard.edu/abs/2019ICRC...36..791S>. Conference Name: 36th International Cosmic Ray Conference (ICRC2019) Place: eprint: arXiv:1909.08750
 19. Sironi, G., Canestrari, R.: The ASTRI SST-2M prototype for the Cherenkov Telescope Array: primary mirror characterization by deflectometry. p. 960304. San Diego, California, United States (2015). DOI 10.1117/12.2188725. URL <http://proceedings.spiedigitallibrary.org/proceeding.aspx?doi=10.1117/12.2188725>
 20. Stringhetti, L.: ASTRI System Requirement Document. Technical Report ASTRI-SPEC-IASFMI-3000-005, INAF-IASFMI (2012)
 21. Watson, J., Flis, S.: Chec camera: pointing calibration (2020, 29 January)
 22. White, R.: CHEC: a Compact High Energy Camera for the Cherenkov Telescope Array. *Journal of Instrumentation* **12**(12), C12059–C12059 (2017). DOI 10.1088/1748-0221/12/12/C12059. URL <https://iopscience.iop.org/article/10.1088/1748-0221/12/12/C12059>